Physically based Probabilistic Rainfall Intensity-Duration (ID) Thresholds for Runoff-Generated Debris Flows

O.R. Francis[1], H. Tang[1], M. Bernard[2]

[1] Section 4.7 Earth Surface Process Modelling, Helmholtz Centre Potsdam, **GFZ** German Research Centre for Geosciences, Potsdam, Germany

[2] Department of Land, Enviroment, Agriculture and Forestry, University of Padua, via dell'Università 16, 35020 Legnaro, PD, Italy

Corresponding author: Oliver Francis (oliver.francis@gfz-potsdam.de)

This manuscript is a preprint uploaded to EarthAirXiv. This preprint has been submitted for publication in Geophysical Research Letters and has not yet been peer-reviewed. We welcome feedback, discussion, and comments at any time.

Physically based Probabilistic Rainfall Intensity-Duration (ID) Thresholds for Runoff-Generated Debris Flows

O.R. Francis[1], H. Tang[1], M. Bernard[2]

[1] Section Earth Surface Process Modelling, Helmholtz Centre Potsdam, **GFZ** German Research Centre for Geosciences, Potsdam, Germany

[2] Department of Land, Enviroment, Agriculture and Forestry, University of Padua, via dell'Università 16, 35020 Legnaro, PD, Italy

Corresponding author: Oliver Francis (oliver.francis@gfz-potsdam.de)

Key Points:

- **Calibration of numerical models using multiple debris flow events reveals the variation of catchment parameters.**
- **Infiltration controls the shape of rainfall intensity-duration thresholds for runoff-generated debris flows in carbonate-dominated catchments**
- **Ensemble of thresholds can estimate the probability of debris flows for a given storm, improving compliance with early warning systems**

Abstract

Runoff-generated debris flows are common hazards in mountainous regions, causing millions of dollars lost and hundreds of casualties yearly. Early warning systems based on rainfall thresholds have been implemented to reduce the impact of these hazards. These thresholds tend to be based on short monitoring periods, which cannot fully capture the varying responses of catchments to rainfall. As a result, the uncertainty of many thresholds is unknown, limiting their usefulness to the general public. We propose a new modelling framework to derive probabilistic rainfall intensity-duration (ID) thresholds from limited observations. We test this framework on a small catchment in the Italian Dolomites to determine probabilistic thresholds for the occurrence of debris flows. Instead of a widely used power-law function, our new rainfall thresholds are a negative exponential function controlled by infiltration capacity. These probabilistic thresholds can help improve early warning system performance by providing additional information to the public.

Plain Language Summary

Debris flows, a very fast and mobile form of landslide, are a common hazard in mountainous areas. To reduce causalities and the economic cost of these hazards it is important that at risk areas have reliable early warning systems. The accuracy of an early warning system is strongly linked to the length of time the area has been monitored. The longer the area has been monitored for, the more debris flows are recorded resulting in more accurate warning systems. However, many debris flow prone regions have limited records of past debris flow events resulting in unreliable warnings. Here we present a new method for producing debris flow forecasts based on short monitoring periods using a numerical model framework. We test this framework on a small simple catchment in the Italian Dolomites with a multi-year record of debris flows. The framework produces many possible scenarios allowing for the probability of a debris flow being triggered to be calculated. These probabilities can be used to produce highly accurate classifications of past debris flow events. A warning system based upon this framework can use these probabilities to provide valuable information to the public enhancing compliance with the system.

1 Introduction

Debris flows, high-speed surges of poorly sorted sediment saturated with water, are one of the most common hazards in mountainous regions (Dowling & Santi, 2014; Fan et al., 2019; Hürlimann et al., 2019; Iverson, 1997). These flows regularly damage local infrastructure such as roads, rail networks, and waterways (Alessio et al., 2021; Bainbridge et al., 2022; Horton et al., 2019; Huang & Fan, 2013; Iverson et al., 2011). Globally between 1950 and 2011, 77,759 casualties were attributed to the direct effects of debris flows, with two events causing over half of the recorded casualties (Dowling & Santi, 2014). The large number of casualties demonstrates the need for accurate early warning systems and engineering measures in debris-flow-impacted areas.

Critical to reducing the economic and human cost of debris flows is the issuing of timely warnings to local communities. These warnings can help ensure homes and businesses are evacuated and transportation routes are closed during times of high risk (Bainbridge et al., 2022; Hürlimann et al., 2019). For effective warnings, an understanding of debris flow triggering conditions is required. Debris flows typically occur in steep mountainous areas during intense rainfall where they can evolve either from landslides or from surface runoff entraining sediment within channels (Bennett et al., 2013; Iverson, 1997; Iverson & George, 2016; Kean et al., 2013; Takahashi, 1981). The triggering conditions of landslide-generated debris flows are relatively well understood and can be estimated through a slope stability analysis (Dietrich & Montgomery, 1998; Guzzetti et al., 2008). Runoff-generated debris flows, on the other hand, are not well understood. Debris flow prone areas have been monitored by a combination of rainfall gauges, passive seismic monitoring, and video camera recording in order to identify their triggering conditions (Badoux et al., 2009; Hürlimann et al., 2019; Kean et al., 2013). However, debris flow initiation is rarely directly observed, and as a result, the exact timing and processes that triggered a particular debris flow are not often known (Benda & Dunne, 1997; Hirschberg et al., 2021; Iverson, 1997; Neely & DiBiase, 2023; Prancevic et al., 2014). Without such information, runoff-triggering debris flows remain challenging to forecast.

An effective early warning system must provide sufficient warning so that communities and businesses have time to organize and prepare (Badoux et al., 2009; Jakob et al., 2012; LeClerc & Joslyn, 2015; Roulston & Smith, 2004). To produce the earliest warning possible most systems rely upon rainfall forecasts (Bernard & Gregoretti, 2021; Berti et al., 2020; Hirschberg et al., 2021; Hürlimann et al., 2019). These systems will issue warnings if the expected rainfall is likely to exceed the intensity of previously recorded debris flow triggering storms (Cannon et al., 2001; Coe et al., 2008; Hürlimann et al., 2019; Staley et al., 2013). The identified critical rainfall intensity is often a function of rainfall duration and is called the rainfall intensity-duration (ID) threshold (Guzzetti et al., 2008; Hirschberg et al., 2021; Iverson, 2000). These thresholds are derived from statistical analysis of observed debris flow triggering rainfall events. Generally, these thresholds are assumed to take the form of a power law function described as:

$$I = \alpha D^{-\beta} \qquad (1)$$

where I represents rainfall intensity, D is storm duration, and α and β are empirical constants (Berti et al., 2020). For these warning systems, the accuracy of this threshold is critical to their success. Poorly performing systems can generate mistrust within the local community through false alarms or by failing to issue a warning of a debris flow potentially leading to casualties (Badoux et al., 2009; LeClerc & Joslyn, 2015; Roulston & Smith, 2004). Determining accurate thresholds can require a large number of recorded debris flows. For example, in the Illgraben catchment in the Swiss Alps, twenty-five debris flow events are required to produce a threshold that accurately classifies 70% of rainfall events (Hirschberg et al., 2021). Twenty-five debris flows are significantly more than have been recorded in almost any other debris flow catchment (Hirschberg et al., 2021; Hürlimann et al., 2019). Therefore, there is a need to produce accurate, testable rainfall ID thresholds from a small number of observations.

Numerical models can be used to reduce the number of recorded debris flow events required for accurate thresholds (Gregoretti & Dalla Fontana, 2008; Tang et al., 2019a). Model-derived thresholds do not require long observational periods to be determined; instead, they can be generated from a model calibrated on a single event. However, thresholds determined by this methodology rarely consider temporal variability in the catchment. The rainfall intensity required to trigger a debris flow has been shown to vary through time, primarily due to changes in the infiltration capacity and sediment availability of the catchment (Guo et al., 2016; Hürlimann et al., 2019; Raymond et al., 2020; Thomas et al., 2021). Considering the natural variability within the numerical model allows for a number of possible scenarios to be generated and probabilistic debris flow forecasts to be derived. Probabilistic forecasts have been shown to increase compliance with warning messages and are more adaptable than traditional empirical thresholds (Beguería, 2006; LeClerc & Joslyn, 2015; Roulston & Smith, 2004).

Here, we present a new modelling framework to derive probabilistic rainfall intensity-duration threshold functions of a small catchment in the Italian Dolomites. With this framework, we calibrate the SWEHR model developed by McGuire et al. (2016, 2017) on four debris flow events to determine the range of possible parameter values. By sampling from this parameter space using a Monte Carlo scheme, we can derive the rainfall ID threshold function of runoff-generated debris flows. Finally, we use this constrained variation to generate an ensemble of one thousand possible rainfall ID thresholds to produce probabilistic thresholds of runoff-generated debris flows.

2 Study area

Our study site is located in the Venetian Dolomites in the north-eastern Italian Alps (Figure 1A), which are composed of a thick fractured dolomitized carbonate rock known as the Dolomia Principale Formation (Berti et al., 2020; Berti & Simoni, 2005; Gregoretti et al., 2016, 2018; Simoni et al., 2020). This lithology forms the steep, picturesque, rocky cliffs which make up the majority of the headwater catchments in the region (Figure 1B). At the foot of these cliffs are post-glacial scree slopes, which are dissected by debris flow channels. Debris flows here are primarily triggered when runoff funneled in from the headwater cliffs mobilizes loose sediment accumulated in the channel (Berti et al., 2020; Gregoretti et al., 2016).

This study focuses on a single catchment, Dimai, located two kilometers north of Cortina d'Ampezzo in Boite Valley. The Dimai catchment is small (97,880m^2) and consists of two main units. The upper headwater part of the catchment (30,440m^2) is formed of the steep (average slope 63^o) western slope of the Pomagagnon massif, and its main channel runs through a forested scree fan (Figure 1B) (Berti et al., 2020; Gregoretti et al., 2016). For this study, we focus on modelling the runoff generation in the headwater catchment to determine its rainfall ID threshold function. The relative simplicity and small size of the headwater catchment make it an excellent location for our study. The lack of significant sediment transport reduces the computational load required for each simulation, allowing a Monte Carlo simulation scheme to be performed. In addition, as the catchment has been monitored and modelled in the past, many major hydrological model parameters have been constrained (Gregoretti et al., 2016; Berti et al., 2020).

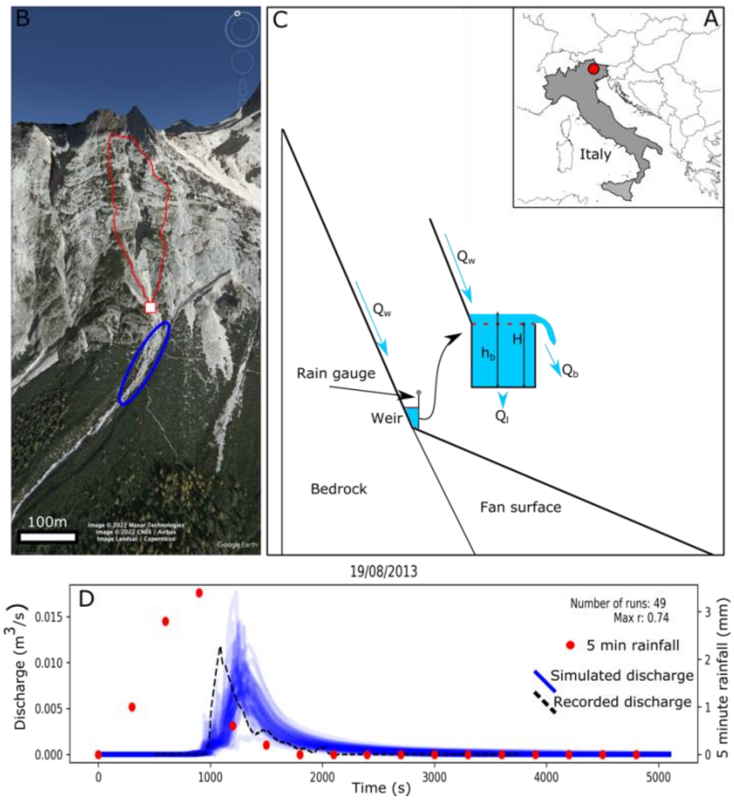

Figure 1: The study area, monitoring setup, and an example of the field observation and model results. (A) The location of the study area. (B) The Dimai headwater catchment (red) shown in Google Earth satellite imagery superimposed on a DEM. Debris flow initiation site is outlined in blue, and the location of the monitoring site is indicated by the white square. (C) A diagram of the monitoring setup adapted from Berti et al., 2020. The monitoring station is located at the base of the headwater catchment and consists of a purpose-built weir, rain gauge, video cameras, and pressure gauges. (D) An example of a calibration exercise, the discharge record is shown as a black dashed line, precipitationis shown as red points, the simulated discharge is shown in blue. There are 49 simulation runs shown here, each with a Pearson's correlation coefficient (r) of greater than 0.5 and a maximum of 0.74.

In 2010, a monitoring station was set up in Dimai to observe debris flow initiation (white box in Figure 1B). This monitoring station used a weir, cameras, and a rain gauge to measure the triggering rainfall and resulting discharge and determine whether a debris flow was triggered. Figure 1C shows the basic setup of the monitoring station. See supplemental information and Berti et al., 2020 for more detail.

The monitoring station was active between 2010 and 2016 and recorded five debris flows, four of which we have the complete discharge and rainfall records required for calibration. All four debris flows occurred during August, highlighting summer convective storms as an important process in triggering debris flow in the area (Berti et al., 2020; Gregoretti et al., 2016). The recorded events are between 15 and 120 minutes long and show steep rising and falling limbs in their discharges, indicating rapid response times and low storage capacity in the catchment (Figure 1D) (Berti et al., 2020). Peak flow depth typically ranges from 20 to 40 cm and can erode several tens of centimeters from the debris flow channel bed. For our study the catchment is represented by one-meter resolution raster DEM derived from a lidar survey performed in October 2011 (Gregoretti et al., 2016).

3 Methodology

3.1 Numerical model

We simulate the runoff response of the catchment using the SWEHR model (McGuire et al., 2016, 2017). The model is comprised of two main components: fluid flow and sediment transport. Since sediment availability is minmal in the headwater catchment, we only focus on calibrating the fluid flow governing equations. Rainfall is converted into runoff via infiltration and interception models before being routed through the catchment using a set of conservation laws with nonlinear shallow water equations (McGuire et al., 2016). Previous studies (Berti et al., 2020; Gregoretti et al., 2016) demonstrated the importance of infiltration in Dimai for controlling the magnitude of the generated runoff. This process is simulated in the model with the Green-Ampt equation. In the model we use separate calibrated parameters for the saturated conductivity of sediment cover and bedrock. We also calibrate Manning's roughness coefficient within the shallow water equations.

The saturated conductivity of the bedrock and sediment controls the rate at which water can infiltrate into the surface (m/s). At higher saturated conductivity values, the water can pass more easily into the subsurface, resulting in a lower runoff volume. Manning's roughness coefficient influences the velocity of the resulting surface runoff. We provide more detail on the Green-Ampt equation in the supplemental information. For more detail on the other parameters of the model, we direct the reader to McGuire et al. (2016).

3.2 Model calibration

We want to identify and constrain any variation within these parameters therefore, we calibrate the model seperately on each of the four recorded discharge events using a Monte Carlo framework. As the interactions and dependencies between the parameters are not known, we use this framework to identify a distribution of possible parameter values for each event. These parameter distributions can then be combined to produce a parameter space representing the catchment variation over the monitoring period.

The framework calibrates the model's parameter space by comparing the simulated and recorded discharge of a known storm. The framework generates one hundred model runs for each recorded storm, each with a unique parameter set. Using Pearson's correlation coefficient, the parameter space is refined by eliminating parameter sets that produce simulations with a coefficient of less than 0.5. The value of 0.5 is chosen as this represents a good correlation between the simulation and recorded event while ensuring some variation in the parameter sets is retained. The correlation coefficient does not capture the magnitude of the discharge, an essential control on debris flow initiation (Gregoretti & Dalla Fontana, 2008; Prancevic et al., 2014; Tang et al., 2019a). Therefore, the framework further refines the parameter space by discarding simulated discharges with a peak of less than 50% of the maximum discharge of the recorded event. The framework then iterates again with a refined parameter space set by a two-standard deviation range of the retained parameter sets. The framework will continue to iterate and refine the parameter space until each rainfall event has 50 retained parameter sets or for five iterations. These iteration limits balance the need to capture the full distribution of the parameter space with computational time. The retained parameter sets for each recorded event are combined to produce the full parameter space for the catchment.

3.3 Hydrodynamic thresholds and Rainfall ID thresholds

Debris flows are triggered when runoff exceeds a critical threshold and rapidly entrains sediment (Gregoretti & Dalla Fontana, 2008; Lamb et al., 2008; Prancevic et al., 2014; Tang et al., 2019b). With our calibrated model and parameter space, we can identify this threshold and determine its relationship to rainfall intensity and duration. This methodology provides us with physically based rainfall ID thresholds that can be tested against known debris flow events (Tang et al., 2019).

Following Tang et al., (2019a), we use two hydrodynamic metrics to calculate the rainfall ID threshold: Shields stress and dimensionless discharge. Shields stress is calculated as:

$$\tau_* = \frac{(\rho_w h S_f)}{(\rho_s - \rho_w) D_{50}} \qquad (2)$$

where ρ_w is the density of water, ρ_s is the density of sediment, h is flow depth, D_{50} is the median grain size, and S_f is the friction slope $S_f = n_0^2(uh^2 + vh^2)h^{\frac{-10}{3}}$, where n_0 is Manning's roughness coefficient and u and v are the velocity in the x and y directions, respectively (Tang et al., 2019a). Shields stress describes the excess stress that acts on grains in the channel pulling it downslope (Takahashi, 1981; Prancevic et al., 2014). The dimensionless discharge is defined as:

$$q_* = \frac{q}{\sqrt{\frac{\rho_s - \rho_w}{\rho_w g}}} \qquad (3)$$

where q is the flow discharge leaving the outlet defined by the product of the water stage and velocity, and g is gravity. τ* and q* are both functions of the channel slope and, therefore, can be compared to other catchments (Gregoretti & Dalla Fontana, 2008; Tang et al., 2019a).

As debris flows are not directly observed within our model domain, we assume the debris flow is triggered by the peak outlet τ* or q*. We derive a distribution of τ* and q* thresholds from the simulations retained from the model calibration. To derive the rainfall ID threshold of the catchment, we need to identify a wide range of rainfall events which can trigger a debris flow. We generate a matrix of 1000 rainfall events bounded by the historical rainfall record of the catchment. The matrix of rainfall events is equally spaced in log space for intensity and duration. The rainfall within these events is normally distributed through time and uniformly across the catchment. Gregoretti et al., (2016) showed that rainfall intensity does not vary significantly across Dimai due to its small size. The framework draws a unique parameter set for each rainfall event and collects the resulting simulated discharge. Finally, the framework calculates τ* and q* of each event. These are compared with the distribution of critical hydrodynamic values to derive the rainfall ID threshold.

With the rainfall matrix and distribution of critical hydrodynamic values, we generate an ensemble of one thousand potential rainfall ID thresholds for the catchment. First, one hundred rainfall events are sampled from the rainfall matrix using a uniform distribution. Next, ten values from the critical hydrodynamic value distributions are chosen to determine possible rainfall ID thresholds. Using an interpolation algorithm (matplotlib.pyplot.tricontour (Hunter, 2007)), a phase space of the hydrodynamic metrics is generated for each sample of rainfall events. The interpolation algorithm then draws a contour of the sampled τ^* or q* values through this space. Finally, the rainfall ID threshold is determined by fitting a negative exponential function to this contour. This shape is chosen based on visual interpretation. In order to test the accuracy of the generated thresholds, we use the F1 accuracy score comparing the predictions of the threshold with the recorded debris flow events (see supplemental information for more details).

4 Results

4.1 Model Calibration

With our Monte Carlo framework, we successfully calibrated the model for all four debris flow events (Figure S1). After running the framework on each rainfall event, 174 calibrated parameter sets were collected and combined to produce a single parameter space. Other than the calibration of the 24th August 2013 debris flow event, the framework retained a minimum of 49 parameter sets. The calibration of the debris flow event on 24th August 2013 ended after five iterations resulting in a low number (11) of retained parameter sets. The resulting parameter space is relatively tight, while saturated conductivity in other locations can vary by several orders of magnitude, our parameter space is limited to a single order (Table S1). From the retained simulations we find that both the Shield's stress and dimensionless discharge critical values for debris flow initiation are log-normally distributed. However, the dimensionless discharge values have a larger standard deviation than the Shields stress values (5.31 v.s. 3.03) (Figure S2).

4.2 Rainfall Intensity-Duration (ID) Thresholds

From our τ_* and q_* phase spaces, we can see that the hydrodynamics of generated runoff are controlled by rainfall duration and intensity (Figure S3). Very short rainfall events generate no runoff, while low-intensity events only produce runoff during long-duration events. Contours of τ_* and q_* close to the minimum duration of runoff generation are steep and then rapidly flatten out to a critical intensity (Figure S3). This relationship is best described as a negative exponential rather than a power law (Figure 2). Our rainfall ID thresholds take the form:

$$I = ae^{-bD} + c \qquad (4)$$

where *I* is the rainfall intensity required to generate the runoff hydrodynamic metric as a function of rainfall duration *D*. *a, b*, and *c* are empirical parameters. Parameter *a* determines where the threshold passes through the y-axis. The *b* parameter controls the rate at which the rainfall intensity changes as a function of the rainfall event duration. And *c* controls the minimum intensity required to exceed the threshold and is strongly correlated with the critical τ_* and q_* chosen to generate the threshold. τ_* consistently produces rainfall ID thresholds with higher intensities than q_*, resulting in a levelling off of the function at a higher point on the y-axis (Figures 2 and S2).

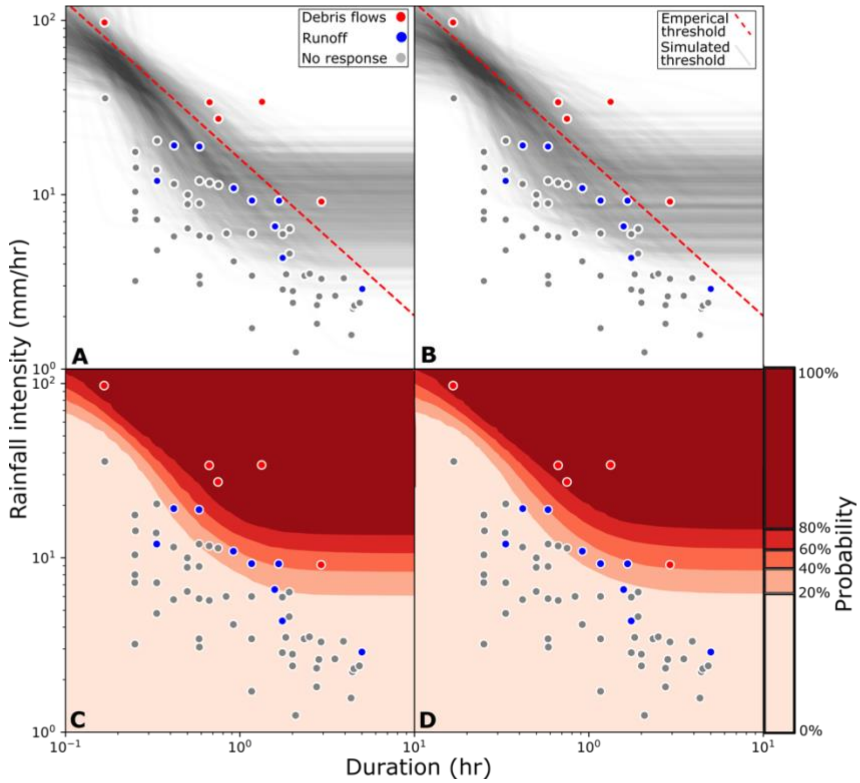

Figure 2: The model-generated rainfall intensity-duration (ID) thresholds. Thresholds generated with q are on the left while τ_* is on the right. In A and B the grey lines are rainfall ID thresholds generated by the Monte Carlo framework. Darker areas indicate parts where many thresholds overlap. The points show the intensity, duration, and runoff response of recorded rainfall events. The red dashed line is the empirical threshold from Berti et al. 2020. C and D show the debris flow probability phase space of the catchment. This spans storms which are above a rainfall ID threshold >80% of the time (dark red) to <20% (pale orange). In all four panels the τ_* thresholds level out at slightly higher intensities than the q_*.*

We combine the ensemble of possible rainfall ID thresholds to estimate the probability of a particular storm triggering a debris flow (Figure 2C and 2D). Storms with high average intensity and long durations are highly likely to be classified as debris flow triggering (top right in Figures 3a and 3b). In contrast, low-intensity and short-duration storms have a very low probability of triggering debris flows (bottom left in Figures 2C and 2D). The contour lines roughly follow power law relationships until the rainstorm duration exceeds one hour. After this duration, the contour lines become nearly flat. The contour maps based on τ_* and q_* are very similar, but the former levels out at higher intensities (~5mm/hr) on average (Figures 2C and 2D).

Finally, we calculate the F_1 scores of probability thresholds to evaluate our modelling framework's ability to classify debris flow triggering rainfall events. We find that probability thresholds close to 0.5 produce the highest F_1 scores (Figure 3). False positives are common at lower thresholds, while higher thresholds produce false negatives resulting in lower F_1 scores (Figure S4). While both τ_* and q_* follow similar trends, there is a slight difference in the peak F_1 scores and probability threshold required to achieve this score. τ_* has a higher maximum F_1 score (0.94 and 0.87) and reaches this at a lower probability threshold (0.48 and 0.59). The minimal difference between the two metrics suggests either can be used to classify debris flow triggering storms in the Dimai catchment.

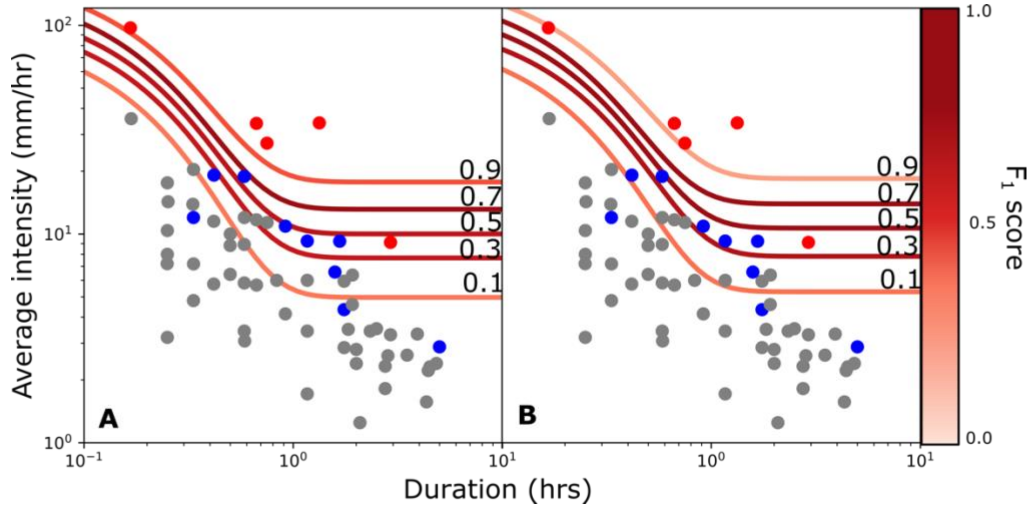

Figure 3. Five probability thresholds colored by their F_1 score A) show thresholds derived from dimensionless discharge and B) are from Shields stress. The probability value of the threshold is shown on the right-hand side of the threshold. Light colors indicate a low F_1 score, while dark colors indicate thresholds with more predictive power. Probability thresholds around 0.5 produce the highest F_1 scores.

5 Discussion

Using a numerical model within a Monte Carlo framework, we derived probabilistic rainfall intensity thresholds for runoff-generated debris flows. The framework used four debris flow events to constrain the variation of a multi-year period within the Dimai catchment. The framework uses this constrained variation and 1000 synthetic rainfall events to derive an ensemble of potential rainfall ID thresholds. This ensemble is then combined to produce probability thresholds, which are tested against the recorded debris flow events. Finally, we find these thresholds are best described by a negative exponential function rather than by a power law, as is commonly assumed (Berti et al., 2020; Guzzetti et al., 2008; Hirschberg et al., 2021; Hürlimann et al., 2019).

The calibration process retains >50 simulations for three of four recorded debris flow events before the iteration limit is reached (Figure S1). For the debris flow event on 24th August 2013, only eleven parameter sets were retained before the iteration limit was reached. Using the identified parameter space, the model cannot consistently reproduce the magnitude of the peak discharge, suggesting infiltration was lower for this event. Infiltration is controlled by two parameters (see supplemental text 2), saturated conductivity and the water content of the subsurface. For each simulation, we assumed that the initial water content was the same; however, an initially wetter catchment could produce more runoff than expected (Dunne, 1983; Mein & Larson, 1973). Five days before 24th August 2013, another debris flow occurred. If it rained during the intervening days or the catchment did not completely drain, a higher initial water content could have occured. This result has been observed in other debris flow catchments, highlighting the importance of considering the variability in hydrological conditions of the catchment in model calibrations (Jakob et al., 2005; Simoni et al., 2020).

The rainfall ID thresholds derived for the Dimai catchment can be separated into two sections, shorter and longer than one-hour duration. Prior to this duration, the thresholds follow a negative power law, while afterwards, the threshold flattens out (Figures 2 and 3). This indicates that, for most rainfall events, the average intensity is the main controlling factor on the stress and discharge of the generated runoff. When controlling for rainfall event intensity, we find that the τ^* and q* of the generated runoff hydrodynamics increase with duration until the duration is close to one hour (Figure S5). After this point, the hydrodynamic metrics become steady and remain close to the selected intensity's median. Lower-intensity storms, however, take longer to reach stability indicating the influence of the initial conditions on the resulting hydrodynamic metrics. From our calibration phase, we know that a particular storm's total volume and peak runoff, and therefore the hydrodynamics, is a function of its saturated conductivity (Figure S6). Therefore, the inflection point from a power law relationship represents the time required for the storm to overcome its initial infiltration conditions. After this inflection point, the resulting hydrodynamic metrics of a storm are only controlled by its intensity. This result further extends the work done by Berti et al. 2020 by showing that infiltration affects not only the y-axis intersection of the threshold but also the overall function used to describe the threshold. Therefore, in areas where large changes in saturated conductivity can occur, such as following wildfires (Raymond et al., 2020; Tang et al., 2019b; Thomas et al., 2021), a change in the threshold function must be considered.

With our probabilistic thresholds, we can classify storms that trigger debris flows with a high degree of accuracy. The maximum F1 score of 0.95 represents a near-perfect classification, though at a relatively low probability threshold of ~0.5 (Figures 4 and S4). Over time the accuracy of this threshold will likely decrease as an increase in the number of false positives is expected. As compliance with a warning system is linked to its performance (LeClerc & Joslyn, 2015; Roulston & Smith, 2004), practitioners should regularly update the thresholds to maintain performance. Our framework improves on existing methodologies in two crucial ways. First, it significantly reduces the time and data required to produce reliable rainfall ID thresholds for debris flow forecasts with reasonable accuracy. This has the potential to greatly improve hazard response in the aftermath of earthquakes and wildfires. Secondly, the framework allows context to be added to warning systems increasing trust in the system. Probabilistic warning thresholds can be easily adjusted for different stakeholders while ensuring compliance rates remain consistent through time.

6 Conclusions

Here we present a new modelling framework to generate probabilistic rainfall intensity-duration thresholds for runoff-generated debris flows. We apply this framework to the Dimai catchment in the Italian Dolomites. By calibrating the numerical model on four separate debris flows events, we constrain the variation in catchment runoff response. This variation is then sampled from to generate many possible rainfall ID thresholds, which are then combined to produce probabilistic classifications for the debris flow record. The thresholds are best described by a negative exponential function indicating the importance of the catchment infiltration for debris flow generation in carbonate catchments. The probabilistic thresholds are highly accurate and can provide vital context to early warning systems, potentially increasing trust and compliance with the warning system.

Acknowledgments

Jens Turowski and Erin Harvey read earlier versions of this manuscript and provided comments which greatly improved the paper.

Open Research

The data from the Dimai monitoring site can be found is publicaly available in the supporting information of Berti et al 2020. The calibration framework, analysis, and visualization Python scripts and notebooks are publically available from https://zenodo.org/record/8163997. Here you can also find the data used to produce the figures in this paper.

References

Alessio, P., Dunne, T., & Morell, K. D. (2021). *Post-wildfire Generation of Debris-flow Slurry by Rill Erosion on Colluvial Hillslopes*. 1–52. https://doi.org/10.1029/2021JF006108

Badoux, A., Graf, C., Rhyner, J., Kuntner, R., & McArdell, B. W. (2009). A debris-flow alarm system for the Alpine Illgraben catchment: Design and performance. *Natural Hazards*, *49*(3), 517–539. https://doi.org/10.1007/s11069-008-9303-x

Bainbridge, R., Lim, M., Dunning, S., Winter, M., Diaz-Moreno, A., Martin, J., Torun, H., Sparkes, B., Khan, M., & Jin, N. (2022). *Detection and forecasting of shallow landslides: Lessons from a natural laboratory*. https://doi.org/10.31223/X52W2R

Beguería, S. (2006). Validation and Evaluation of Predictive Models in Hazard Assessment and Risk Management. *Natural Hazards*, *37*(3), 315–329. https://doi.org/10.1007/s11069-005-5182-6

Benda, L., & Dunne, T. (1997). Stochastic forcing of sediment routing and storage in channel networks. *Water Resources*, *33*(12), 2865–2880.

Bennett, G. L., Molnar, P., McArdell, B. W., Schlunegger, F., & Burlando, P. (2013). Patterns and controls of sediment production, transfer and yield in the Illgraben. *Geomorphology*, *188*, 68–82. https://doi.org/10.1016/j.geomorph.2012.11.029

Bernard, M., & Gregoretti, C. (2021). The Use of Rain Gauge Measurements and Radar Data for the Model-Based Prediction of Runoff-Generated Debris-Flow Occurrence in Early Warning Systems. *Water Resources Research*, *57*(3). https://doi.org/10.1029/2020WR027893

Berti, M., Bernard, M., Gregoretti, C., & Simoni, A. (2020). Physical Interpretation of Rainfall Thresholds or Runoff-Generated Debris Flows. *Journal of Geophysical Research: Earth Surface*, *125*(6), 1–25. https://doi.org/10.1029/2019JF005513

Berti, M., & Simoni, A. (2005). Experimental evidences and numerical modelling of debris flow initiated by channel runoff. *Landslides*, *2*(3), 171–182. https://doi.org/10.1007/s10346-005-0062-4

Cannon, S. H., Kirkham, R. M., & Parise, M. (2001). Wildfire-related debris-flow initiation processes, Storm King Mountain, Colorado. *Geomorphology*, *39*(3–4), 171–188. https://doi.org/10.1016/S0169-555X(00)00108-2

Coe, J. A., Kinner, D. A., & Godt, J. W. (2008). Initiation conditions for debris flows generated by runoff at Chalk Cliffs, central Colorado. *Geomorphology*, *96*(3–4), 270–297. https://doi.org/10.1016/j.geomorph.2007.03.017

Dietrich, W. E., & Montgomery, D. R. (1998). SHALSTAB: a digital terrain model for mapping shallow landslide potential. *National Council of the Paper Industry for Air and Stream Improvement Technical Report, February 1998*, *LVIII*(1976), 29.

Dowling, C. A., & Santi, P. M. (2014). Debris flows and their toll on human life: A global analysis of debris-flow fatalities from 1950 to 2011. *Natural Hazards*, *71*(1), 203–227. https://doi.org/10.1007/s11069-013-0907-4

Dunne, T. (1983). Relation of field studies and modeling in the prediction of storm runoff. *Journal of Hydrology*, *65*(1–3), 25–48. https://doi.org/10.1016/0022-1694(83)90209-3

Fan, X., Scaringi, G., Korup, O., West, A. J., van Westen, C. J., Tanyas, H., Hovius, N., Hales, T. C., Jibson, R. W., Allstadt, K. E., Zhang, L., Evans, S. G., Xu, C., Li, G., Pei, X., Xu, Q., & Huang, R. (2019). Earthquake-Induced Chains of Geologic Hazards: Patterns, Mechanisms, and Impacts. *Reviews of Geophysics*. https://doi.org/10.1029/2018RG000626

Gregoretti, C., & Dalla Fontana, G. (2008). The triggering of debris flow due to channel-bed failure in some alpine headwater basins of the Dolomites: Analyses of critical runoff. *Hydrological Processes*, *22*(13), 2248–2263. https://doi.org/10.1002/hyp.6821

Gregoretti, C., Degetto, M., Bernard, M., & Boreggio, M. (2018). The debris flow occurred at ru secco creek, venetian dolomites, on 4 august 2015: Analysis of the phenomenon, its characteristics and reproduction by models. *Frontiers in Earth Science*, *6*(November), 1–20. https://doi.org/10.3389/feart.2018.00080

Gregoretti, C., Degetto, M., Bernard, M., Crucil, G., Pimazzoni, A., De Vido, G., Berti, M., Simoni, A., & Lanzoni, S. (2016). Runoff of small rocky headwater catchments: Field observations and hydrological modeling. *Water Resources Research*, *52*(10), 8138–8158. https://doi.org/10.1002/2016WR018675

Guo, X., Cui, P., Li, Y., Ma, L., Ge, Y., & Mahoney, W. B. (2016). Intensity-duration threshold of rainfall-triggered debris flows in the Wenchuan Earthquake affected area, China. *Geomorphology*, *253*, 208–216. https://doi.org/10.1016/j.geomorph.2015.10.009

Guzzetti, F., Peruccacci, S., Rossi, M., & Stark, C. P. (2008). The rainfall intensity-duration control of shallow landslides and debris flows: An update. *Landslides*, *5*(1), 3–17. https://doi.org/10.1007/s10346-007-0112-1

Hirschberg, J., Badoux, A., McArdell, B. W., Leonarduzzi, E., & Molnar, P. (2021). Evaluating methods for debris-flow prediction based on rainfall in an Alpine catchment. *Natural Hazards and Earth System Sciences*, *21*(9), 2773–2789. https://doi.org/10.5194/nhess-21-2773-2021

Horton, A. J., Hales, T. C., Ouyang, C., & Fan, X. (2019). Identifying post-earthquake debris flow hazard using Massflow. *Engineering Geology*, *258*. https://doi.org/10.1016/j.enggeo.2019.05.011

Huang, R., & Fan, X. (2013). The landslide story. *Nature Geoscience*, *6*(5), 325–326. https://doi.org/10.1038/ngeo1806

Hunter, J. D. (2007). Matplotlib: A 2D graphics environment. *Computing in Science & Engineering*, *9*(3), 90–95. https://doi.org/10.1109/MCSE.2007.55

Hürlimann, M., Coviello, V., Bel, C., Guo, X., Berti, M., Graf, C., Hübl, J., Miyata, S., Smith, J. B., & Yin, H. Y. (2019). Debris-flow monitoring and warning: Review and examples. *Earth-Science Reviews*, *199*(October), 102981. https://doi.org/10.1016/j.earscirev.2019.102981

Iverson, R. M. (1997). The Physics of Debris Flows. *Reviews of Geophysics*, *35*(3), 245–296.

Iverson, R. M. (2000). Landslide triggering by rain infiltration. *Water Resources Research, 36*(7), 1897–1910. https://doi.org/10.1029/2000WR900090

Iverson, R. M., & George, D. L. (2016). Modelling landslide liquefaction, mobility bifurcation and the dynamics of the 2014 Oso disaster. *Geotechnique, 66*(3), 175–187. https://doi.org/10.1680/jgeot.15.LM.004

Iverson, R. M., Reid, M. E., Logan, M., LaHusen, R. G., Godt, J. W., & Griswold, J. P. (2011). Positive feedback and momentum growth during debris-flow entrainment of wet bed sediment. *Nature Geoscience*, *4*(2), 116–121. https://doi.org/10.1038/ngeo1040

Jakob, M., Bovis, M., & Oden, M. (2005). The significance of channel recharge rates for estimating debris-flow magnitude and frequency. *Earth Surface Processes and Landforms*, *30*(6), 755–766. https://doi.org/10.1002/esp.1188

Jakob, M., Owen, T., & Simpson, T. (2012). A regional real-time debris-flow warning system for the District of North Vancouver, Canada. *Landslides*, *9*(2), 165–178. https://doi.org/10.1007/s10346-011-0282-8

Kean, J. W., McCoy, S. W., Tucker, G. E., Staley, D. M., & Coe, J. A. (2013). Runoff-generated debris flows: Observations and modeling of surge initiation, magnitude, and frequency. *Journal of Geophysical Research: Earth Surface*, *118*(4), 2190–2207. https://doi.org/10.1002/jgrf.20148

Lamb, M. P., Dietrich, W. E., & Venditti, J. G. (2008). Is the critical shields stress for incipient sediment motion dependent on channel-bed slope? *Journal of Geophysical Research: Earth Surface, 113*(2), 1–20. https://doi.org/10.1029/2007JF000831

LeClerc, J., & Joslyn, S. (2015). The Cry Wolf Effect and Weather-Related Decision Making: Crying Wolf and Weather-Related Decision Making. *Risk Analysis*, *35*(3), 385–395. https://doi.org/10.1111/risa.12336

McGuire, L. A., Kean, J. W., Staley, D. M., Rengers, F. K., & Wasklewicz, T. A. (2016). Constraining the relative importance of raindrop- and flow-driven sediment transport mechanisms in postwildfire environments and implications for recovery time scales. *Journal of Geophysical Research: Earth Surface*, *121*(11), 2211–2237. https://doi.org/10.1002/2016JF003867

McGuire, L. A., Rengers, F. K., Kean, J. W., & Staley, D. M. (2017). Debris flow initiation by runoff in a recently burned basin: Is grain-by-grain sediment bulking or en masse failure to blame? *Geophysical Research Letters*, *44*(14), 7310–7319. https://doi.org/10.1002/2017GL074243

Mein, R. G., & Larson, C. L. (1973). Modeling infiltration during a steady rain. *Water Resources Research*, *9*(2), 384–394. https://doi.org/10.1029/WR009i002p00384

Neely, A. B., & DiBiase, R. A. (2023). Sediment controls on the transition from debris flow to fluvial channels in steep mountain ranges. *Earth Surface Processes and Landforms*, *n/a*(n/a), 1–20. https://doi.org/10.1002/esp.5553

Prancevic, J. P., Lamb, M. P., & Fuller, B. M. (2014). Incipient sediment motion across the river to debris-flow transition. *Geology*, *42*(3), 191–194. https://doi.org/10.1130/G34927.1

Raymond, C. A., McGuire, L. A., Youberg, A. M., Staley, D. M., & Kean, J. W. (2020). Thresholds for post-wildfire debris flows: Insights from the Pinal Fire, Arizona, USA. *Earth Surface Processes and Landforms*, *45*(6), 1349–1360. https://doi.org/10.1002/esp.4805

Roulston, M. S., & Smith, L. A. (2004). The Boy Who Cried Wolf Revisited: The Impact of False Alarm Intolerance on Cost–Loss Scenarios. *Weather and Forecasting*, *19*(2), 391–397. https://doi.org/10.1175/1520-0434(2004)019<0391:TBWCWR>2.0.CO;2

Simoni, A., Bernard, M., Berti, M., Boreggio, M., Lanzoni, S., Stancanelli, L. M., & Gregoretti, C. (2020). Runoff-generated debris flows: Observation of initiation conditions and erosion–deposition dynamics along the channel at Cancia (eastern Italian Alps). *Earth Surface Processes and Landforms*, *45*(14), 3556–3571. https://doi.org/10.1002/esp.4981

Staley, D. M., Kean, J. W., Cannon, S. H., Schmidt, K. M., & Laber, J. L. (2013). Objective definition of rainfall intensity-duration thresholds for the initiation of post-fire debris flows in southern California. *Landslides*, *10*(5), 547–562. https://doi.org/10.1007/s10346-012-0341-9

Takahashi, T. (1981). Debris flow. *Annual Review of Fluid Mechanics*, *13*, 57–77. https://doi.org/10.1146/annurev.fl.13.010181.000421

Tang, H., McGuire, L. A., Rengers, F. K., Kean, J. W., Staley, D. M., & Smith, J. B. (2019a). Developing and Testing Physically Based Triggering Thresholds for Runoff-Generated Debris Flows. *Geophysical Research Letters*, *46*(15), 8830–8839. https://doi.org/10.1029/2019GL083623

Tang, H., McGuire, L. A., Rengers, F. K., Kean, J. W., Staley, D. M., & Smith, J. B. (2019b). Evolution of Debris-Flow Initiation Mechanisms and Sediment Sources During a Sequence of Postwildfire Rainstorms. *Journal of Geophysical Research: Earth Surface*, *124*(6), 1572–1595. https://doi.org/10.1029/2018JF004837

Thomas, M. A., Rengers, F. K., Kean, J. W., McGuire, L. A., Staley, D. M., Barnhart, K. R., & Ebel, B. A. (2021). Postwildfire Soil-Hydraulic Recovery and the Persistence of Debris

Flow Hazards. *Journal of Geophysical Research: Earth Surface*, *126*(6), 1–25.
https://doi.org/10.1029/2021JF006091

Geophysical Research Letters

Supporting Information for

Physically based Probabilistic Rainfall Intensity-Duration (ID) Thresholds for Runoff-Generated Debris Flows

Oliver Francis[1], Hui Tang[1], Martino Bernard[2]

1. Section 4.7 Earth Surface Process Modelling, Helmholtz Centre Potsdam, **GFZ** German Research Centre for Geosciences, Potsdam, Germany
2. Department of Land, Enviroment, Agriculture and Forestry, University of Padua, via dell'Università 16, 35020 Legnaro, PD, Italy

Contents of this file

Introduction

Here you will find the supplemental text, figures, and table referred to in the main text of the paper. Supporting Text S1 provides further information on the monitoring station at Dimai, in particular we provide more detail on how discharge is measured. Supporting Text S2 provides more information on the Green-Ampt infiltration model. Supporting Text S3 details the F_1 score used to measure the accuracy of the thresholds derived by the modelling framework.

Text S1.

Here, we briefly describe the monitoring set up at Dimai, as shown in Figure 1C. For a more complete description and photos of the monitoring setup we direct the reader to Gregoretti et al., 2016 and Berti et al., 2020. The monitoring station consisted of a weir and two rain gauges (one at the weir one at the top of the headwater catchment) and was supported by video cameras for confirmation of debris flow events. The weir was used to measure the discharge leaving the headwater catchment during rainfall events while the rain gauges captured the intensity and duration of the rainfall event. Rainfall intensity was measured using a standard tipping-bucket rain gauge with a sensitivity of 0.2mm. The rain gauge starts recording once the rainfall intensity exceeds 0.2mm/hr. The duration of the rainfall event is defined by the length of time the rainfall remains above this threshold. The rainfall intensity is summed and recorded for five-minute intervals.

Discharge exiting the headwater catchment was calculated by recording the change in volume of a stilling basin downstream of a purpose-built weir (Figure 1C). The discharge was estimated by calculating the change in volume of the basin through time:

$$Q_w(t) = \frac{dV_b}{dt} + Q_l + Q_b \qquad (1)$$

where Q_w is the volume of water in the basin as a function of time (t), dV_b/dt is the change in the volume of water in the basin, Q_b is the discharge of water leaving the basin above the weir wall, and Q_l is the discharge from the incompletely sealed basin base (~0.6×10^{-4} m^3/s). The height of the water in the stilling basin was measured with a pressure sensor located in its base. The water height is then combined with the height and width of the weir to determine Q_b:

$$Q_b = C_D B_E \sqrt{2g}(h_b - H)^{\frac{3}{2}} \qquad (2)$$

Here C_D is a discharge coefficient (0.4). B_E is the effective weir width ($1.55 - 0.1(h_b$-H)), where h_b is the height of the water table, and H is the height of the weir wall. The temporal resolution of these measurements is five minutes, the same as the rain gauges. When rainfall events are recorded, video cameras are activated to determine whether a debris flow is triggered.

Text S2.

Infiltration has been shown to be an important control on the final discharge exiting the headwater basin at Dimai. Within the SWEHR model, infiltration is modelled by the Green-Ampt equation which includes the calibratable parameter, saturated conductivity of the surface. As this model has a strong impact on our simulation results, we describe it here. Infiltration (I_c) is calculated by;

$$I_c = K_s \frac{Z_f + h_f + h}{Z_f} \qquad (3)$$

where K_s is saturated conductivity, Z_f is the wetting front depth, hf is the wetting front capillary pressure head, and h is the pressure the runoff depth acting on the saturated zone below the surface. Saturated conductivity is the speed at which the water can pass through the saturated medium. Z_f is the depth from the surface, which marks the transition between the saturated and unsaturated zones. h_f describes the pressure on the water resulting from the suction of the unsaturated pore spaces below. Z_f is calculated as:

$$Z_f = \frac{I_d}{\theta_s - \theta_i} \qquad (4)$$

where I_d is the cumulative infiltrated depth, θ_s and θ_i are the saturated and initial volumetric water content, respectively. Within the SWEHR model, we can provide separate saturated conductivities for bedrock and sediment. Hence, we need to calibrate both saturated conductivities and Manning's roughness coefficient. The initial ranges of parameters are constrained from previous work on the catchment and can be viewed in Table S1.

Text S3.

In order to test the accuracy of our modelling framework, we compare our probabilistic thresholds with the historical record of rainfall events from the monitoring station. Here, we use the F_1 score, which is defined as the harmonic mean of a given threshold's precision and recall:

$$F_1 = \frac{R+P}{2} \qquad (5)$$

Precision is calculated by:

$$P = \frac{TP}{TP+FP} \qquad (6)$$

where TP is the number of true positives, i.e., a storm that has been correctly classified as debris flow triggering, and FP is the number of false positives, i.e., a storm that has been incorrectly predicted as debris flow triggering. The recall is calculated by

$$R = \frac{TP}{TP+FN} \qquad (7)$$

where FN is the number of false negatives, storms incorrectly classified as not triggering a debris flow. The final F_1 score varies between zero and one, where one is a perfect classification with no false classifications, and zero represents no predictive power. By calculating the F_1 score for different probabilities, we can determine the predictive power of the framework.

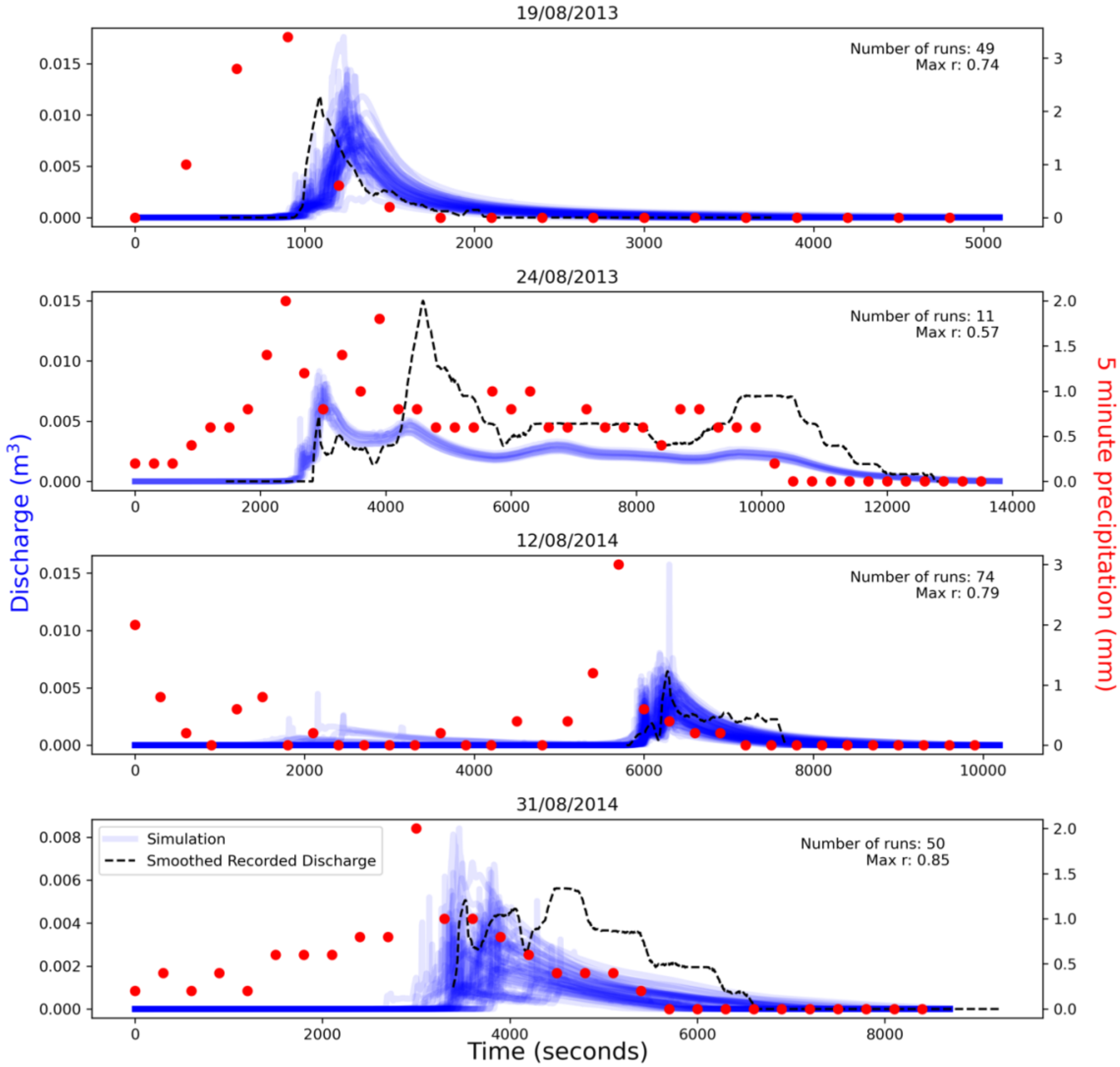

Figure S1. Results of the calibration process for the four debris flow events. For each event, we show the recorded discharge as a black dashed line and the recorded precipitation as red dots. The simulations resulting from the calibration process are shown in blue, and areas where many cases overlap are shown as darker. We only show the simulations that are deemed well calibrated, i.e., they have a Pearson's Correlation coefficient (r) greater than 0.5 and a maximum discharge greater than half the recorded discharge. In each panel, we list the number of runs shown in the figure and the maximum Pearson's correlation coefficient of these runs (r).

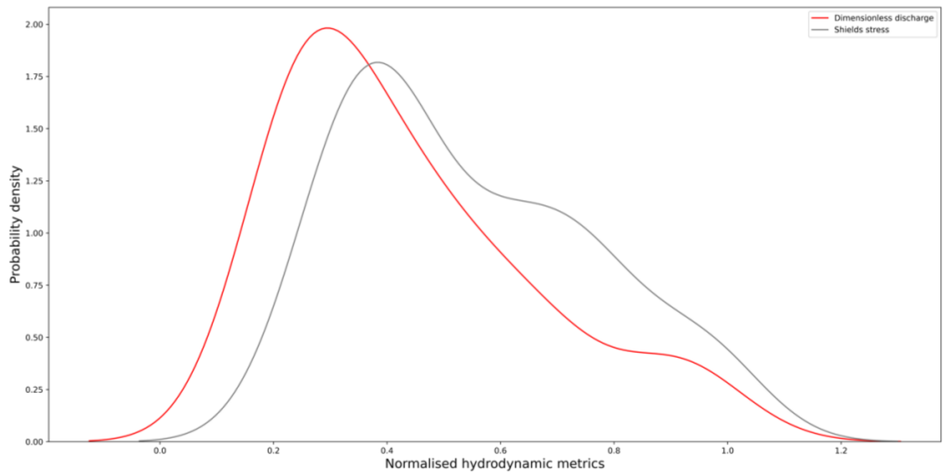

Figure S2. Kernel density plots of the distributions of Dimensionless discharge and Shields stress derived from the maximum values of the well-calibrated cases. The values are normalized by dividing the distribution by its maximum value.

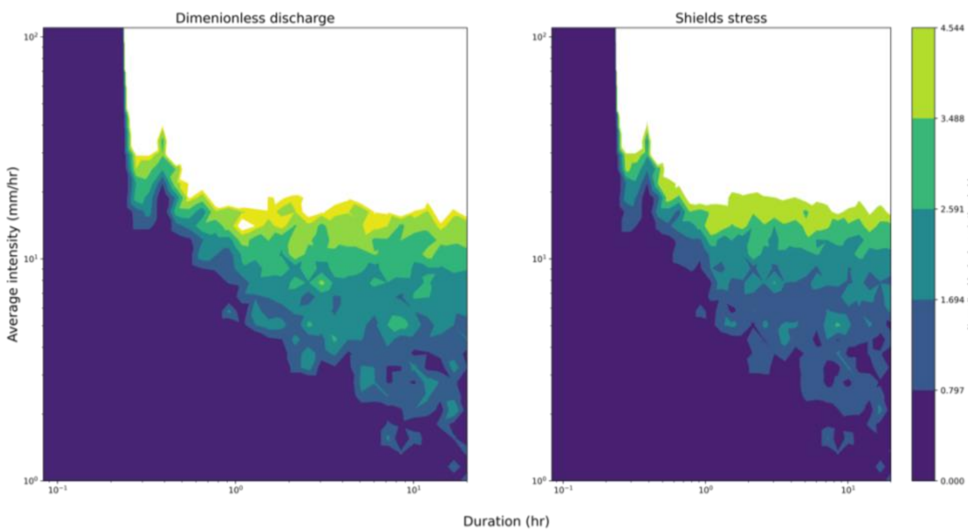

Figure S3. Contour plots of dimensionless discharge and Shields stress derived from the thousand simulated rainfall events using the tricountorf Python package. The color bar is normalized by the median value of each hydrodynamic metric. White areas produce hydrodynamic metrics greater than two standard deviations from the median critical value used to derive the rainfall intensity-duration thresholds. The contours are complex due to the variation in input parameters used to derive the simulations.

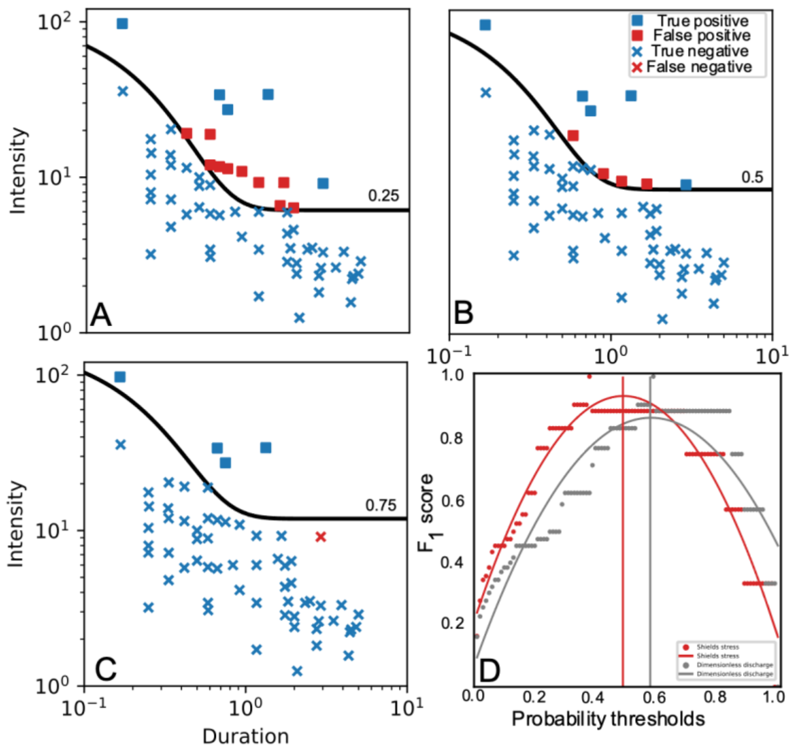

Figure S4. The numbers of false predictions vary depending on the probability threshold chosen as a classifier. In A, a probability threshold of 0.25 is used which results in a high number of false positives. While in C, a probability threshold of 0.75 is used, and a false negative is produced. This results in a parabolic shape of F1 scores as shown in D (Red is Shields stress, and grey is dimensionless discharge).

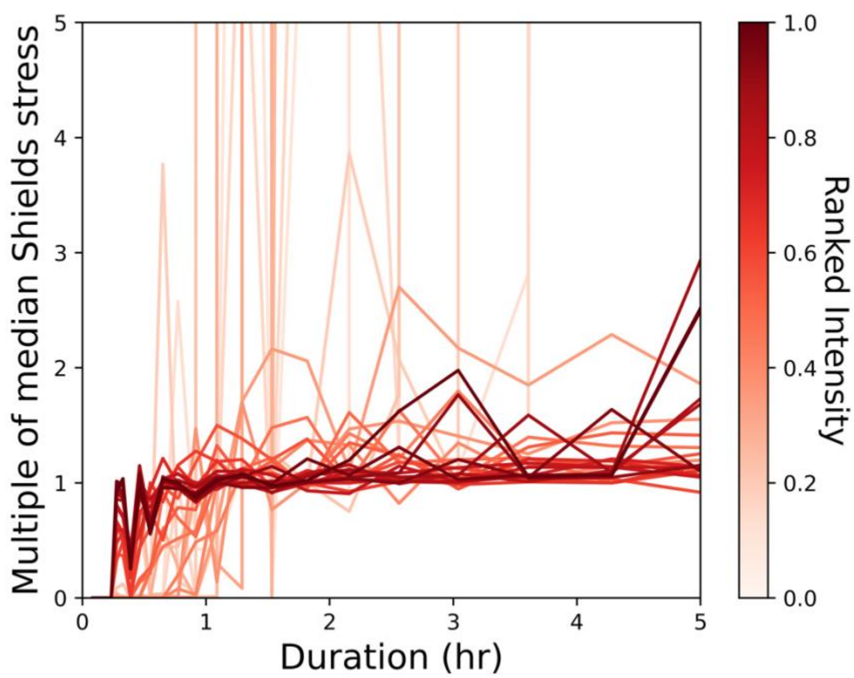

Figure S5. Rainfall events are grouped by their intensity which is then ranked so that the darkest red lines have the highest intensity. The Shields stress generated by each storm is normalized by the median for all storms with that intensity. All intensity groups tend to their median by an hour in duration. Light (low intensity) groups are highly variable.

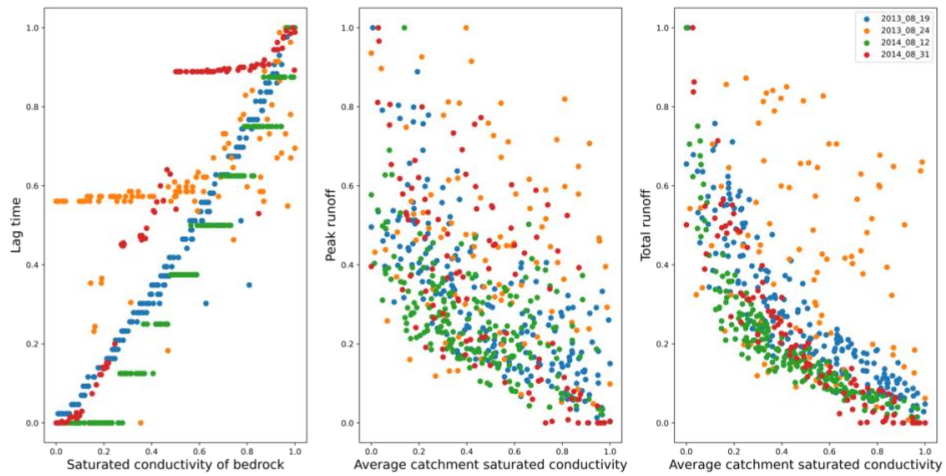

Figure S6. Correlations between the lag time, peak runoff, and total runoff volume and saturated conductivity for the calibration debris flow events. All values are normalized using the min-max method.

Event Date	Saturated conductivity of sediment (Ks) (m/s)	Saturated conductivity of bedrock (Ks) (m/s)	Manning's roughness coefficient (n)
Initial range	1×10^{-7} - 1×10^{-5}	1×10^{-7} - 1×10^{-5}	0.1 – 0.5
19/08/2013	1.41×10^{-7} – 9.68×10^{-6}	1.19 – 9.33×10^{-7}	0.15 – 0.19
24/08/2013	3.02 – 8.22×10^{-7}	5.14 – 8.74×10^{-7}	0.18 – 0.20
12/08/2014	7.15×10^{-7} – 7.6×10^{-6}	1.08 – 9.95×10^{-7}	0.15 – 0.20
31/08/2014	3.80×10^{-7} – 8.12×10^{-6}	1.07 – 9.96×10^{-7}	0.15 – 0.20
Combined	2.38×10^{-7} – 4.13×10^{-6}	2.57 – 7.63×10^{-7}	0.16 – 0.19

Table S1. The Initial and calibrated parameter spaces for each event and the final combined space.